INTERNATIONAL JOURNAL FOR NUMERICAL METHODS IN FLUIDS
Int. J. Numer. Meth. Fluids 2000; **33**: 313–332

Robustness versus accuracy in shock-wave computations

Jérémie Gressier[a,*,1] and Jean-Marc Moschetta[b,2]

[a] *ONERA DMAE BP 4025, 31055 Toulouse cedex 4, France*
[b] *Ecole Nationale Supérieure de l'Aéronautique et de l'Espace, 31400 Toulouse, France*

SUMMARY

Despite constant progress in the development of upwind schemes, some failings still remain. Quirk recently reported (Quirk JJ. A contribution to the great Riemann solver debate. *International Journal for Numerical Methods in Fluids* 1994; **18**: 555–574) that approximate Riemann solvers, which share the exact capture of contact discontinuities, generally suffer from such failings. One of these is the odd–even decoupling that occurs along planar shocks aligned with the mesh. First, a few results on some failings are given, namely the carbuncle phenomenon and the *kinked Mach stem*. Then, following Quirk's analysis of Roe's scheme, general criteria are derived to predict the odd–even decoupling. This analysis is applied to Roe's scheme (Roe PL, Approximate Riemann solvers, parameters vectors, and difference schemes, *Journal of Computational Physics* 1981; **43**: 357–372), the Equilibrium Flux Method (Pullin DI, Direct simulation methods for compressible inviscid ideal gas flow, *Journal of Computational Physics* 1980; **34**: 231–244), the Equilibrium Interface Method (Macrossan MN, Oliver. RI, A kinetic theory solution method for the Navier–Stokes equations, *International Journal for Numerical Methods in Fluids* 1993; **17**: 177–193) and the AUSM scheme (Liou MS, Steffen CJ, A new flux splitting scheme, *Journal of Computational Physics* 1993; **107**: 23–39). Strict stability is shown to be desirable to avoid most of these flaws. Finally, the link between marginal stability and accuracy on shear waves is established.

KEY WORDS: shock waves; stability analysis; upwind schemes

1. INTRODUCTION

One of the most common failings in compressible Euler computations is the *carbuncle* phenomenon, which appears in the computation of blunt-body problems. This pathological behavior has been commonly encountered in many high-speed flows, particularly when the bow shock is aligned with grid lines. In some situations, the carbuncle phenomenon is so badly developed that the flow field downstream is very far from any engineering prediction or experimental data. Another failing, called the *kinked Mach stem*, occurs in unsteady

* Correspondence to: ONERA DMAE BP 4025, 31055 Toulouse cedex 4, France.
[1] E-mail: gressier@onecert.fr
[2] E-mail: moscheta@supaero.fr

Received December 1998
Revised July 1999

computations where shocks propagate along a wall. Before analyzing the way these failings appear, some results are given on classical upwind schemes such as Roe's scheme [19] or Osher's scheme [13] and more recent schemes such as the AUSM scheme [10] and EFMO [12]. These schemes have been selected because of their shock-capturing capabilities which make them well-suited for the computation of high-speed flows.

The AUSM variant which has been used is one of the first variants proposed in the literature, named as the *Mach splitting* version, and labeled AUSM-M in the present study. Additional computations have shown that AUSM-M produces nearly the same results as the recent AUSM+ variant [8].

EFMO results from Coquel's Hybrid Upstream Splitting technique [2], which has been applied to the Equilibrium Flux Method (EFM) proposed by Pullin [16] and to Osher's scheme. Proposed by Moschetta [12] it shares the robustness of EFM and the accuracy on shear and contact waves provided by Osher's method.

In the first section, two classical failings of these schemes are described and various numerical explanations are reported and discussed. In Section 3, the odd–even decoupling problem proposed by Quirk [17] is computed using various upwind methods, followed by a general linear stability analysis. Following Quirk [17] this linear stability analysis is applied to Roe's scheme in Section 4 including the effect of Harten's entropy fix. In Section 5, the linear stability analysis is applied to two kinetic schemes: EFM and EIM, taking advantage of the differentiability of their numerical functions. In Section 6, the particular behavior of the AUSM-M scheme (Mach-splitting variant) is analyzed and its damping properties are compared with the ones from Roe's scheme. Finally, in Section 8, the stability analysis is applied to the linearized form of a generic upwind scheme. The link between marginal stability and accuracy on contact discontinuities is mathematically established. Furthermore, viscous computations are presented to quantify the effects of natural viscosity on these failings.

2. TWO CLASSICAL FAILINGS

Among well known failings in compressible Euler computations, some of them are strongly connected to the computation of shock waves. The most famous example is the carbuncle phenomenon, which occurs in the bow shock ahead of blunt-body shapes in supersonic flows. Unexpected behavior of shock waves can also appear in unsteady computations. One such behavior is the *kinked Mach stem*, detailed in the following section.

According to recent results [4,7,17] most Riemann solvers (Roe, Osher) produce spurious solutions, while Flux Vector Splitting (FVS) schemes yield a physical computation of shock waves. Numerical results show that the Hybrid Upwind Splitting (HUS) technique [2], which restores the resolution of contact discontinuities, also makes the flaw appear [4].

2.1. The carbuncle phenomenon

Although FVS schemes are not affected by this problem, they cannot be used efficiently in the framework of the Navier–Stokes equations since their intrinsic dissipative mechanism tends to artificially broaden boundary layers. First, computations of the hypersonic flow around a

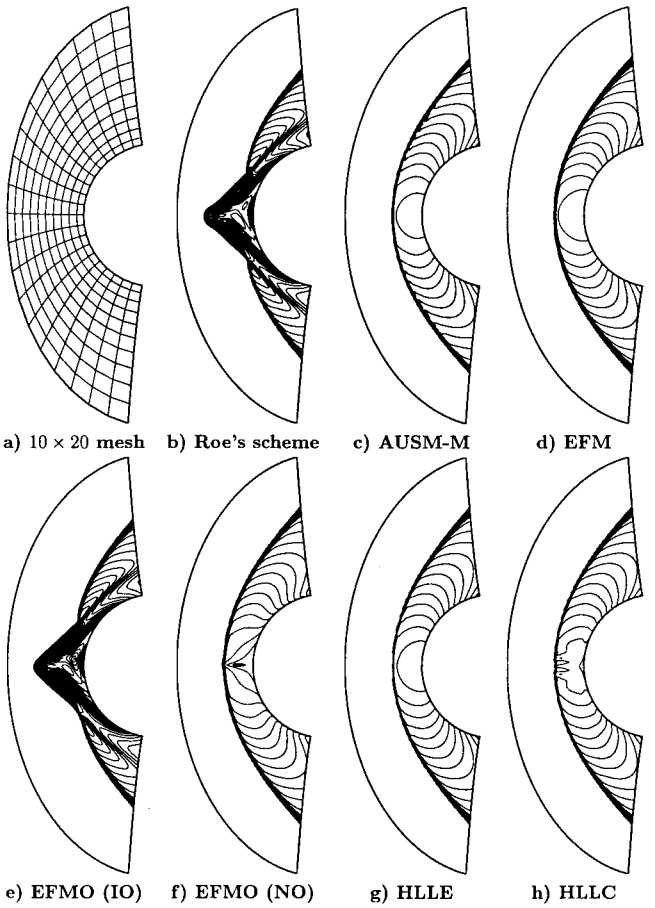

Figure 1. 80×160 computations of a forward-facing cylinder, $M_\infty = 10$, temperature contours.

forward-facing cylinder are presented. The freestream Mach number is 10. The computational mesh is composed of 80×160 cells. In Figure 1(a), one cell over eight is presented for clarity.

First reported by Peery and Imlay [15] with Roe's scheme, the carbuncle phenomenon is all the more likely to show that the mesh is aligned with the detached bow shock. It consists of a spurious stagnation point which moves the shock upstream along the symmetry axis. The carbuncle phenomenon is highly grid-dependent, but does not require a large number of points to appear. In certain cases, the numerical solution converges toward a steady solution including the carbuncle phenomenon even though the residuals have come down to zero machine accuracy. This means that, *for a fixed space resolution*, an unphysical solution of the steady discretized Euler equations can be obtained with a consistent and stable conservative method. This conclusion is not in contradiction with the Lax–Wendroff theorem [6] since

when the grid is even more refined, unphysical solutions are more and more perturbed and eventually the computation fails to converge toward a steady solution.

According to the results shown in Figure 1, AUSM-M, HLLE [3] and EFM are the only schemes, among those included in this study, which naturally provide a physical calculation around the stagnation line (Figure 1(c–d)). However, Pandolfi and D'Ambrosio [14] showed computations where the AUSM-M family yields perturbed contours downstream of the shock. These results are not surprising since the carbuncle phenomenon is highly grid-dependent.

The EIM scheme was not plotted: its lack of robustness prevents any attempt to compute this case without reaching negative pressures.

Osher's scheme blows up in the first time steps for both natural (NO) and inverse ordering (IO) of the eigenvalues because of the severity of the initial freestream conditions. Steady state solutions can still be reached by using another suitable scheme during the first time steps.

A steady solution can also be reached with Roe's scheme by applying Harten's entropy fix [5,7]. In principle, this fix should not be applied to the multiple eigenvalue $\lambda = u$, because that would just be a convenient way to introduce a minimal amount of dissipation on shear waves. Indeed, the mathematical justification to modify the eigenvalues is simply to enforce a second-law principle to the Euler equations in order to get rid of expansion shocks that might otherwise appear. Thus, the entropy fix should only be applied on eigenvalues associated with sonic points such as $\lambda = u - a$ and $\lambda = u + a$. If this is done, Roe's scheme still develops the carbuncle problem. However, if this fix is also applied to $\lambda = u$ the carbuncle disappears provided that a minimum value of Harten's parameter has been used. Yet, there are two drawbacks associated with this extended correction: (1) the exact resolution of shock waves is lost, i.e. the entropy fix introduces an intermediate point in the resolution and (2) boundary layers are significantly broadened when using a typical value for Harten's entropy fix function, i.e. the exact resolution of contact waves is also lost. This entropy fix has also been discussed by Quirk [17] and Sanders *et al.* [20] who proposed an extension of this fix.

Because it is based upon the HUS technique, which provides the exact resolution of contact discontinuities, the EFMO scheme suffers from the same flaw as Osher's scheme: the inverse ordering develops the same unphysical protuberance as Roe's scheme. With the natural ordering, the shape of the bow shock is not as badly affected, but the stagnation line remains perturbed.

The fact that the EFM scheme is not affected by the carbuncle phenomenon suggests that a link should exist between the exact resolution of contact discontinuities (which has been restored in the EFMO scheme) and this flaw. This is confirmed by results obtained using upwind schemes belonging to the HLL family. The restoration of the contact surface proposed by Toro *et al.* [21] and Batten *et al.* [1] in the HLL Riemann solver makes the flaw appear (HLLC scheme, Figure 1(h)), while the HLLE scheme [3] is not affected (Figure 1(g)). Similar results with others members of the HLL Riemann solvers family are presented in Reference [14].

Based on numerical experiments, Liou [9] proposed a criterion on the mass flux dependencies to pressure difference. Similarly, Xu [23] proposed a more detailed explanation for the apparition of this anomalous phenomenon in the Riemann solvers family. On the other hand, the features of linear instability have been recently studied by Sanders *et al.* [20] and Robinet *et al.* [18]

2.2. The kinked Mach stem

Another pathological behavior is the kinked Mach stem, which occurs on double Mach reflection (DMR) cases. The test consists of a $M_s = 5.5$ Mach number shock impinging a 30° ramp. The principal Mach stem can be severely kinked and an unphysical triple point appears. Although this problem is an unsteady case, this failing seems to be similar to the carbuncle phenomenon since it appears when insufficient dissipation cannot counteract transverse perturbations.

Roe and Osher's schemes both suffer from this failing (Figure 2(b, d and e)). However, EFM and AUSM-M schemes (Figure 2(c) and Figure 3(a)) do not seem to be affected. Nevertheless, density contours do not have the same aspect at the wall. Although the AUSM-M scheme does not seem to fail on this grid [9], density contours look similar to those obtained with schemes

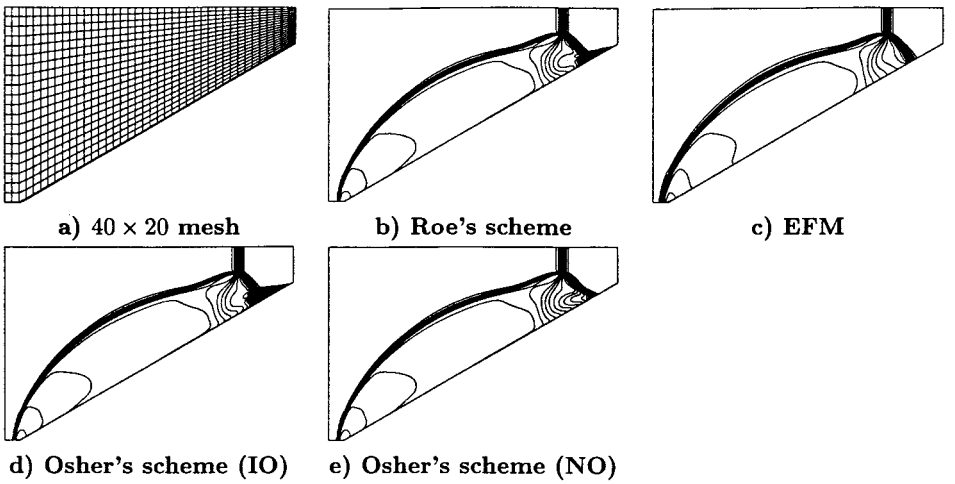

Figure 2. 200 × 100 computations of a DMR case, density contours.

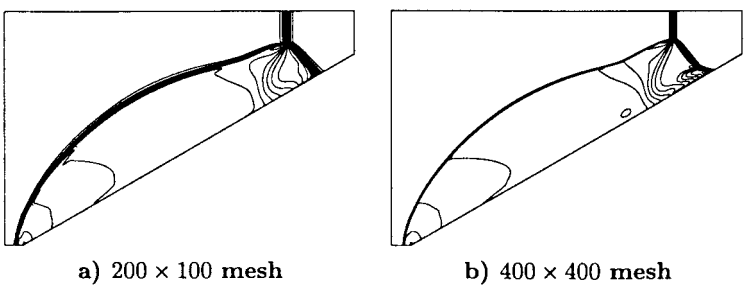

Figure 3. Coarse and refined computations of a DMR case, AUSM-M scheme, density contours.

which suffer from the kinked Mach stem. A more refined computation (Figure 3(b)) shows that the AUSM-M scheme can produce the kinked Mach stem as well, whereas the EFM scheme does not, even at this level of grid refinement. This is consistent with the results of blunt-body calculations where grid refinement has been observed to promote the unphysical solution.

3. ODD–EVEN DECOUPLING AND QUIRK'S TEST

Quirk [17] reported another insidious failing which can occur in very high resolution simulations. It is an odd–even decoupling problem in which perturbations grow along planar shocks which are aligned with the mesh. Quirk proposed to test and analyze this shortcoming with a new case: the propagation of a planar shock in a duct where the centerline is perturbed.

3.1. Description and numerical results

The computational mesh has 800×20 cells for a 40×1 length unit duct. The centerline of the mesh is perturbed following:

$$y_{i,j_{\text{mid}}} = y_{j_{\text{mid}}} + (-1)^i \cdot 10^{-6} \tag{1}$$

The shock wave is traveling with a Mach number $M_s = 6$. The shock wave Mach number M_s is defined as u_s/a_r where u_s is the speed of the traveling wave and a_r is the sound speed where the flow is at rest.

Results are shown in Figure 4. As the shock propagates downstream, perturbations grow until the shock completely breaks down. In Figure 4, several snapshots have been superimposed on the same duct to observe the different schemes temporal evolution. In the case of successful computations, straight shapes of the shock can be observed at $x = 12$, 18 and 24 length units. Otherwise, perturbations grow, the shock shape is dramatically perturbed and its velocity slightly increases.

The Roe, Osher, Macrossan EIM [11] and EFMO schemes fail to remain stable in this case. AUSM-M and EFM schemes provide the same sharp profile. However, a closer analysis shows that transverse oscillations of the order of the perturbation appear in AUSM-M scheme profiles while no such oscillations occur with EFM.

It is noticed that better results are obtained with Osher and EFMO schemes when using the NO of eigenvalues rather than the IO originally proposed by Osher. In Quirk's test case, the AUSM-M scheme is the only one which provides both vanishing dissipation on contact discontinuities and robustness to odd–even decoupling.

Although the entire study deals with first-order schemes, it is important to note that the extension to second-order computations would not cure these pathological behaviors. Some comparisons between first-order and second-order computations are provided in Figure 5 for several schemes. The second-order accuracy is achieved by a classical MUSCL [22] extension. Reconstructions are calculated using primitive variables and the *minmod* limiter. Numerical results show that the second-order extension does not cure the odd–even decoupling (Figure

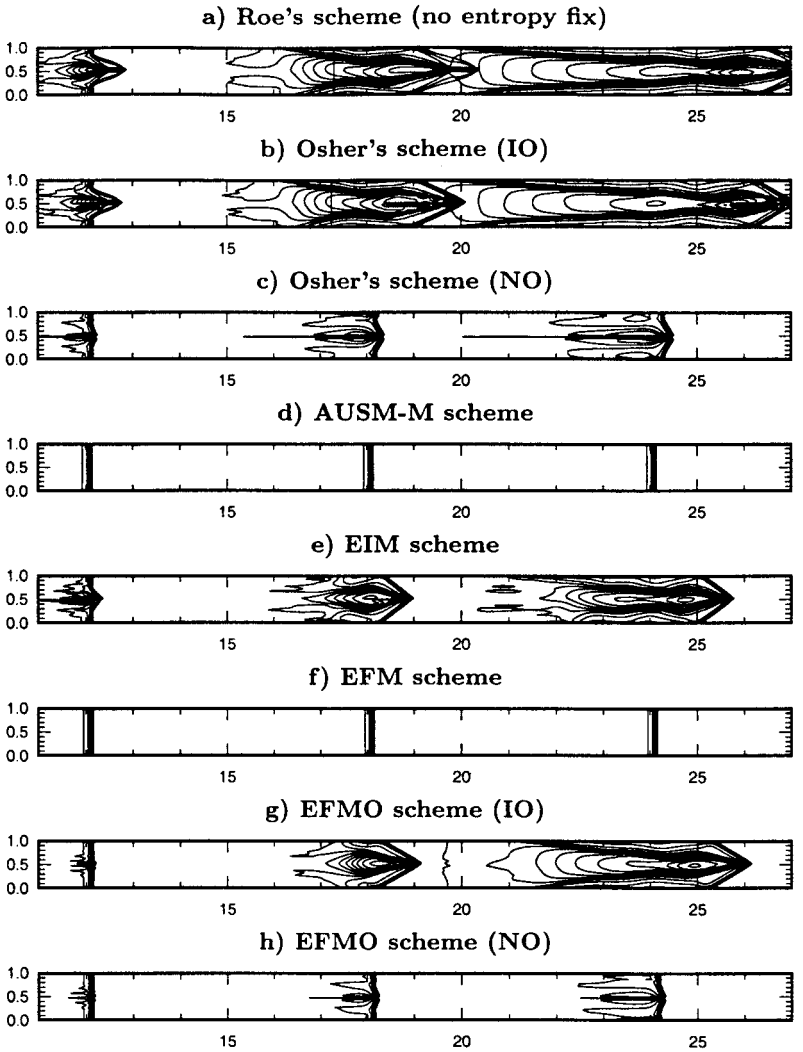

Figure 4. Quirk's test results, Mach number contours.

5(a–b)). Although the shock shape seems to be less perturbed, the computed solution still remains unacceptable. On the other hand, the MUSCL extension does not trigger the failing either (Figure 5(c–d)). These results support the choice of only considering first-order schemes in the following.

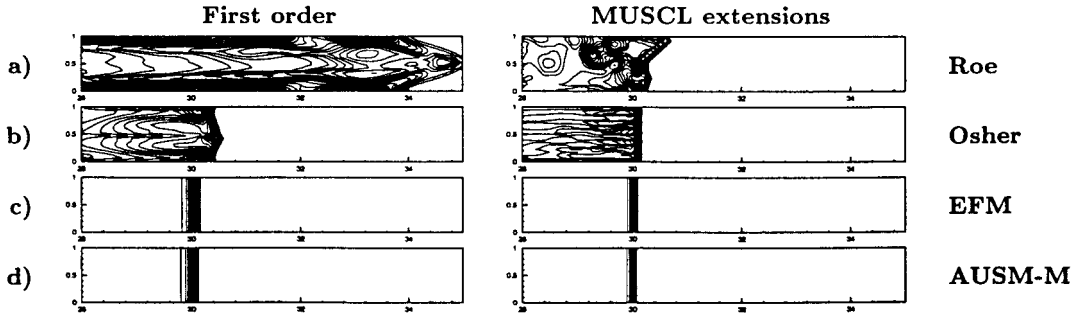

Figure 5. Quirk's test results, MUSCL extensions, density contours.

3.2. Stability analysis

To find some criteria in order to predict odd–even decoupling, a linear stability analysis is applied to the 2D inviscid equations for a uniform flow, the state vector of this flow is denoted $\mathscr{U}_0$. This state represents a longitudinal flow whose density, sound speed and Mach number are ρ_0, a_0 and M_0 respectively.

According to numerical experiments, sawtooth-like perturbations only develop in transverse planes. Hence, it is assumed that streamwise fluxes are always balanced. The conservation equation then becomes:

$$\mathscr{U}_j^{n+1} = \mathscr{U}_j^n - \sigma[G_{j+1/2} - G_{j-1/2}] \tag{2}$$

where $\sigma = \Delta t/\Delta y$ and $G_{j+1/2}$ denotes the numerical flux function $G(\mathscr{U}_j, \mathscr{U}_{j+1})$.

The aim of Von Neumann analysis is to calculate an amplification matrix $\mathbb{A}$ which rules the behavior of the error vector $\delta\mathscr{U}_j^n = \mathscr{U}_j^n - \mathscr{U}_0$ following the amplification relation $\delta\mathscr{U}_j^{n+1} = \mathbb{A} \cdot \delta\mathscr{U}_j^n$. The spectral radius of $\mathbb{A}$, $\rho(\mathbb{A})$, i.e. the maximum of the absolute value of the eigenvalues of $\mathbb{A}$, provides a stability criterion.

By assuming $\delta\mathscr{U}_{j-1} = -\delta\mathscr{U}_j = \delta\mathscr{U}_{j+1}$ the balance of transverse fluxes can be linearized into:

$$G_{j+1/2} - G_{j-1/2} = \mathbb{G} \cdot \delta\mathscr{U}_j \tag{3}$$

where $\mathbb{G}$ is a matrix that only depends on $\mathscr{U}_0$. After linearization, Equation (2) then becomes:

$$\delta\mathscr{U}^{n+1} = (\mathbb{I} - \sigma\mathbb{G}) \cdot \delta\mathscr{U}^n \tag{4}$$

The amplification matrix $\mathbb{A}$ can then be expressed as $\mathbb{A} = \mathbb{I} - \sigma\mathbb{G}$. Hence, if $\mathbb{G}$ has some zero eigenvalues $\lambda_{\mathbb{G}}$, the scheme is then marginally stable as corresponding $\mathbb{A}$ eigenvalues are unity for any Courant–Friedrich–Lewy (CFL) number. Otherwise, the strict stability condition $|\lambda_{\mathbb{A}}| < 1$ leads to a CFL-like condition by developing $\lambda_{\mathbb{A}} = 1 - \sigma\lambda_{\mathbb{G}}$:

$$|\lambda_{\mathbb{A}}|^2 = (1 - \sigma \mathrm{Re}(\lambda_{\mathbb{G}}))^2 + (\sigma \mathrm{Im}(\lambda_{\mathbb{G}}))^2 < 1 \tag{5a}$$

$$1 + \sigma(\sigma|\lambda_{\mathbb{G}}|^2 - 2\mathrm{Re}(\lambda_{\mathbb{G}})) < 1 \tag{5b}$$

$$\sigma|\lambda_{\mathbb{G}}|^2 - 2\mathrm{Re}(\lambda_{\mathbb{G}}) < 0 \tag{5c}$$

Hence, the following CFL-like condition provides a linearly stable scheme:

$$\sigma < \frac{2\mathrm{Re}(\lambda_{\mathbb{G}})}{|\lambda_{\mathbb{G}}|^2} \tag{6}$$

It should be pointed out that this criterion just comes from a stability analysis of a constant flow. The shock relations have not been considered in this approach.

4. ROE'S SCHEME ANALYSIS

Quirk [17] has already proposed an analysis of Roe's scheme failure. The same assumptions were used concerning streamwise fluxes, but only pressure and density perturbations were considered.

In the present study, a similar analysis is performed using all components to describe the perturbed state vector. The interface flux of Roe's scheme may be written as:

$$G_{j+1/2} = \frac{1}{2}(\mathscr{G}_j + \mathscr{G}_{j+1}) - \frac{1}{2}\sum_k \alpha^k_{j+1/2}|\tilde{\lambda}^k_{j+1/2}|\tilde{e}^k_{j+1/2} \tag{7}$$

where $\tilde{\lambda}^k$ are the eigenvalues, α^k the corresponding wave strengths and $\tilde{e}^k$ the corresponding right eigenvectors. More details and full expressions can be found in Reference [19].

4.1. Stability of odd–even perturbations

Since wave strengths are of the order of the perturbed quantities, the eigenvalues and eigenvectors which depend on Roe averaged state can be evaluated with the constant state $\mathscr{U}_0$. These assumptions lead to the following properties:

$$\mathscr{G}_{j-1} = \mathscr{G}_{j+1} \tag{8a}$$

$$\alpha^k_{j-1/2} = -\alpha^k_{j+1/2} \tag{8b}$$

$$\tilde{\lambda}^k_{j-1/2} = \tilde{\lambda}^k_{j+1/2} \tag{8c}$$

$$\tilde{e}^k_{j-1/2} = \tilde{e}^k_{j+1/2} \tag{8d}$$

The conservation Equation (2) can be developed and yields:

$$\delta \mathscr{U}_j^{n+1} = \delta \mathscr{U}_j^n - 2v_y \begin{pmatrix} (\delta p^n/\tilde{a}^2) \\ \mathscr{U}_0(\delta p^n/\tilde{a}^2) \\ \rho_0\, \delta v^n \\ H_0(\delta p^n/\tilde{a}^2) \end{pmatrix} \tag{9}$$

where $v_y = \sigma a_0$ can be interpreted as a CFL number. To extract an amplification matrix, Equation (9) can be expressed (assuming $a_0 \simeq \tilde{a}$) as:

$$\begin{pmatrix} \delta p \\ \delta u \\ \delta v \\ \delta p \end{pmatrix}^{n+1} = \begin{pmatrix} 1 & 0 & 0 & -2v_y/a_0^2 \\ 0 & 1 & 0 & 0 \\ 0 & 0 & 1-2v_y & 0 \\ 0 & 0 & 0 & 1-2v_y \end{pmatrix} \begin{pmatrix} \delta \rho \\ \delta u \\ \delta v \\ \delta p \end{pmatrix}^{n} \tag{10}$$

This result shows that density and streamwise velocity errors are marginally stable since they are associated with an amplification factor equal to one. Then, these perturbations are totally driven by source terms which are not modeled here. In Quirk's problem, source terms come from unbalanced fluxes along the perturbed centerline. The present analysis only describes the development of an initial perturbation.

Marginal stability confirms numerical experiments where odd–even decoupling does not depend on the CFL number. This implies that the marginal stability property is an intrinsic mechanism directly dependent on the flux function definition.

4.2. Effects of the extended entropy fix

In the same way as it does for the carbuncle and the kinked Mach stem failings, an extension of the true entropy fix can cure the odd–even decoupling failing. The extension consists of applying this fix to linear waves which govern shear and contact discontinuities. But this has no mathematical or physical justification: it is just a convenient method to add a minimal amount of artificial dissipation. None of the true entropy fix (where the fix is only applied to $v \pm a$ eigenvalues) can cure Roe's failure.

A similar stability analysis is performed with Roe's scheme using the extended entropy fix. Absolute values of the eigenvalues of Equation (7) are replaced by Harten's function [5] in which Harten's parameter δ_0 is evaluated from the spectral radius according to $\delta_0 = \delta(|v_0| + a_0)$ where δ is a problem-dependent tunable parameter. The present analysis is not affected by the use of a more elaborate form of δ_0 [7] since δ_0 comes directly into the amplification matrix.

Referring to the previous analysis of the original version of Roe scheme (see Section 4.1), when the entropy fix is applied, the calculation now consists of replacing the eigenvalue $|v_0|$ by δ_0. After the same calculation which has led to Equation (10), pressure and transverse velocity perturbations can be shown to remain stable under a CFL condition as observed in the latter case. Amplification factors of density and streamwise velocity perturbations now become:

$$\left(1 - \frac{2\delta_0}{a_0} v_y\right) \tag{11}$$

instead of 1 as in the latter analysis of Roe's original scheme (without any fix).

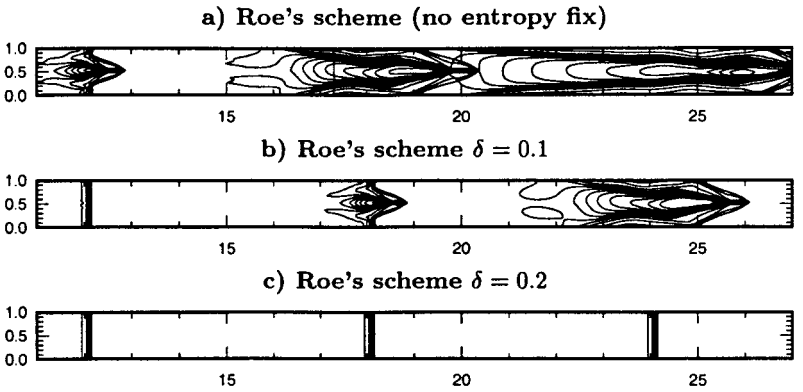

Figure 6. Effects of the extended entropy fix, Mach number contours.

Owing to the extended entropy fix, Roe's scheme becomes stable under a CFL condition. Surprisingly, numerical results of Figure 6 show that a threshold ($\delta \simeq 0.2$) is necessary to remove the odd–even decoupling problem. Results of Figure 6(b) show the limits of the present analysis since linear stability condition is satisfied for $\delta = 0.1$, i.e. $\rho(\mathbb{A}) < 1$, while results still indicate instability. At this point, further analysis taking into account the shock structure and the contribution of streamwise fluxes is certainly needed.

Nevertheless, the stability analysis carried out for both versions of Roe's scheme suggests that marginal stability is not a desirable property for upwind schemes.

5. EFM AND EIM SCHEMES ANALYSIS

Both EFM and EIM schemes interface flux share infinite differentiability with respect to their left and right states. Therefore, amplification matrix $\mathbb{A}$ can be directly calculated as a function of the Jacobian matrices of the interface flux $G(\mathscr{U}_L, \mathscr{U}_R)$. Conservation Equation (2) is linearized and $\mathbb{A}$ is evaluated via $\mathbb{G}$ as:

$$\mathbb{G} = 2\left(\frac{\partial G}{\partial \mathscr{U}_L} - \frac{\partial G}{\partial \mathscr{U}_R}\right)_{\mathscr{U}_0} \tag{12}$$

5.1. EFM scheme

The EFM scheme amplification matrix is evaluated following Equation (12). Expressions remain intricate but, by computing its determinant, matrix $\mathbb{G}$ can be shown to have no zero eigenvalue. Hence, the EFM scheme is strictly stable under a CFL condition. This confirms the good damping properties observed in numerical experiments.

5.2. EIM scheme

The same method can be used to evaluate the EIM scheme amplification matrix.

It can be written via $\mathbb{G}$ as:

$$\mathbb{G} = \sqrt{\frac{2}{\gamma\pi}} \begin{pmatrix} \Theta & \dfrac{-\bar{\gamma}M_0}{a_0} & 0 & \dfrac{\bar{\gamma}}{a_0^2} \\ M_0 a_0 \Theta & -\bar{\gamma}M_0^2 & 0 & \dfrac{\bar{\gamma}M_0}{a_0} \\ 0 & 0 & \gamma+1 & 0 \\ \dfrac{a_0^2\Theta\Psi}{\gamma-1} & -\gamma M_0 a_0 \Psi & 0 & \gamma\Psi \end{pmatrix} \tag{13}$$

where $\bar{\gamma} = \gamma(\gamma-1)$, $\Theta = 1 + \gamma((\gamma-1)/2)M_0^2$ and $\Psi = 1 + ((\gamma-1)/2)M_0^2$.

Because of column vectors dependencies, $\mathbb{G}$ yields two zero eigenvalues. Indeed, the second column is equal to $-a_0 M_0$ times the fourth and the first is $a^2\Theta/\bar{\gamma}$ times the fourth. Obviously, a third one is $\sqrt{2/\gamma\pi}(\gamma+1)$. The trace of matrix $\mathbb{G}$ provides the fourth eigenvalue $\sqrt{2/\gamma\pi}(\gamma+1)$. Finally, the complete set of eigenvalues is:

$$[0 \quad ; \quad 0 \quad ; \quad \sqrt{2/\gamma\pi}(\gamma+1) \quad ; \quad \sqrt{2/\gamma\pi}(\gamma+1)] \tag{14}$$

Hence, $\mathbb{A}$ has two eigenvalues equal to one and, consequently, the EIM scheme is marginally stable. This is consistent with the numerical results (Figure 4(e)).

6. AUSM-M SCHEME ANALYSIS

Like Roe's scheme, AUSM-M interface flux expressions are not differentiable around the constant state $\mathscr{U}_0$. Properties of upwind functions in AUSM-M scheme are used. For odd–even perturbations, one has:

$$\delta M_{j+1} = -\delta M_j = \delta M_{j-1} \tag{15}$$

Hence, by first-order approximations,

$$M_{j+1/2} = M^+(\delta M_j) + M^-(\delta M_{j+1}) = 0 \tag{16a}$$

$$M_{j-1/2} = M^+(\delta M_{j-1}) + M^-(\delta M_j) = 0 \tag{16b}$$

$$p_{j+1/2} = p^+(\delta M_j) + p^-(\delta M_{j+1}) = 2p^+(\delta M_j) \tag{16c}$$

$$p_{j-1/2} = p^+(\delta M_{j-1}) + p^-(\delta M_j) = 2p^-(\delta M_j) \tag{16d}$$

Convective terms disappear in the conservation Equation (2). The pressure term is the only one left. It influences the transverse momentum equation following:

$$\rho_0 a_0 \delta M_j^{n+1} = \rho_0 a_0 \delta M_j^n - 2\sigma[p_j^+ - p_j^-] \tag{17}$$

In the AUSM-M scheme, $p^\pm$ can be linearized as $p^\pm = 1/2p(1 \pm 3/2M)$. This leads to the amplification matrix:

$$\begin{pmatrix} \delta\rho \\ \delta u \\ \delta v \\ \delta p \end{pmatrix}^{n+1} = \begin{pmatrix} 1 & 0 & 0 & 0 \\ 0 & 1 & 0 & 0 \\ 0 & 0 & 1 - \dfrac{3}{\gamma} v_y & 0 \\ 0 & 0 & 0 & 1 \end{pmatrix} \begin{pmatrix} \delta\rho \\ \delta u \\ \delta v \\ \delta p \end{pmatrix}^n \tag{18}$$

The AUSM-M scheme is therefore also marginally stable. Nevertheless, numerical experiments indicate that it does not suffer from odd–even decoupling. This result points out that marginal stability cannot be considered as a criterion to predict odd–even decoupling since it can lead either to methods which are prone to develop the odd–even decoupling problem or to methods which will not amplify nor damp perturbations, such as the AUSM-M scheme.

7. DAMPING PROPERTIES

Although the AUSM-M and EFM schemes do not have the same amplification matrix since the EFM is strictly stable (under a CFL condition) and the AUSM-M is marginally stable, none of them suffer from odd–even decoupling in Quirk's test. Nevertheless, the EFM is expected to have better damping properties. This is confirmed by the following results.

The moving shock is computed using Roe's scheme until it has covered 9 length units ($t = 1.5$). This unsteady solution is then used as an initial condition for the AUSM-M, EFM or Roe's scheme as if the computation had not been interrupted. The three cases are represented in Figure 7, where the first slice ($x = 9$) comes from the same computation. First, Figure 7 shows that the shock profile has already been greatly perturbed while using Roe's scheme (Figure 7, $x = 9$). Transverse snapshots show that density profiles suffer from oscillations of 20 per cent magnitude (Figure 8). The three computations of Figure 7 show the damping properties of these three schemes:

- an entire computation with Roe's scheme fail since the shock profile has blown up at $x = 15$;
- the AUSM-M seems to cope with these initial conditions: perturbations are not amplified but remain at 20 per cent magnitude (Figure 9) in the third slice (Figure 7(b), $x = 15$);

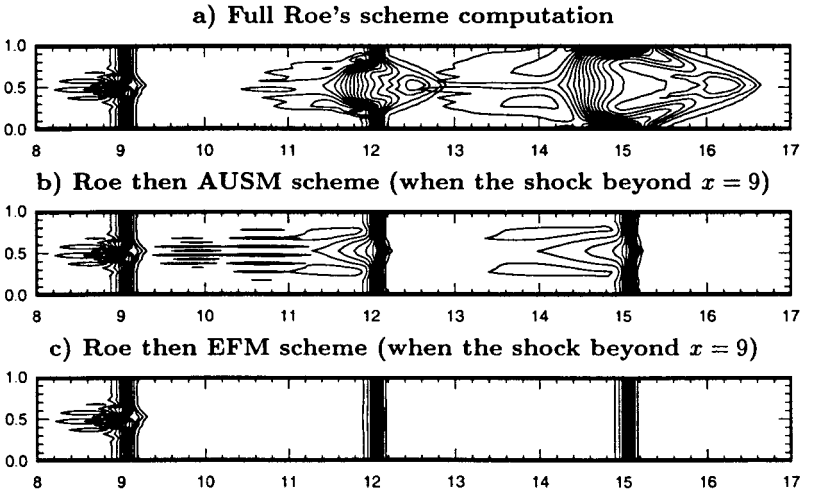

Figure 7. Computations from a spurious solution, density contours.

- the EFM scheme proves to have good damping properties since perturbation magnitudes have decreased from 20 to 0.4 per cent (Figure 10) in the third slice (Figure 7(c), $x = 15$, with magnified density scales).

This suggests that marginal stability of the AUSM-M scheme might lead to difficulties in more severe situations as has already been illustrated by the refined computation of the DMR case (Figure 3(b)).

8. MARGINAL STABILITY AND ACCURACY ON SHEAR WAVES

This section aims at exhibiting a relationship between the exact resolution of contact discontinuities and the marginal stability of upwind schemes. First, a general form of a central scheme with second-order matrix dissipation is considered and the stability analysis is applied. Then, results are extended to all first-order upwind schemes.

The numerical flux of a central scheme with matrix dissipation of second-order writes:

$$G(\mathscr{U}_L, \mathscr{U}_R) = \frac{1}{2}(\mathscr{G}_L + \mathscr{G}_R) - \frac{1}{2} A_D(\mathscr{U}_L, \mathscr{U}_R) \cdot (\mathscr{U}_R - \mathscr{U}_L) \tag{19}$$

Note that Roe's scheme belongs to this family by choosing $A_D(\mathscr{U}_L, \mathscr{U}_R) = |(\partial \mathscr{G}/\partial \mathscr{U})(\tilde{\mathscr{U}})|$ where $\tilde{\mathscr{U}}$ is Roe's average state of $\mathscr{U}_L$ and $\mathscr{U}_R$. The stability analysis is applied to this family of schemes. The balance of fluxes writes:

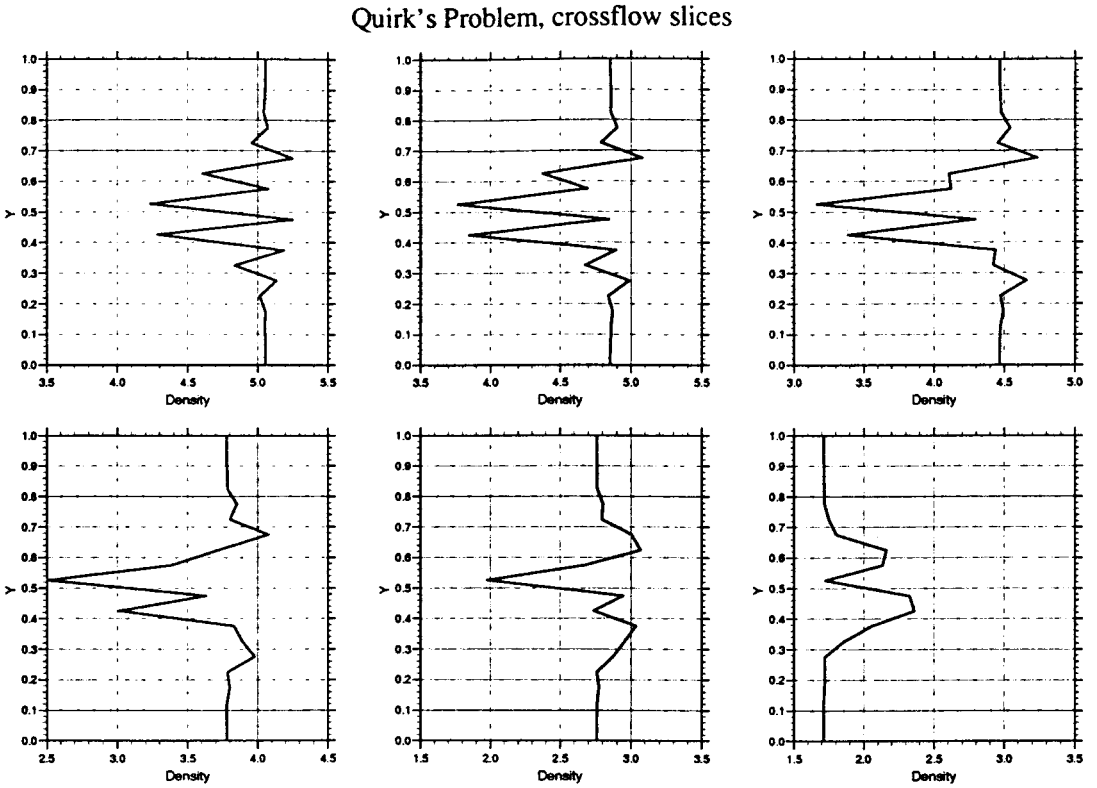

Figure 8. Density profiles within the shock for successive vertical grid lines around $x = 9$, Roe's scheme.

$$G(\mathscr{U}_j, \mathscr{U}_{j+1}) - G(\mathscr{U}_{j-1}, \mathscr{U}_j) = \frac{1}{2}[\mathscr{G}_j + \mathscr{G}_{j+1} - \mathscr{G}_{j-1} - \mathscr{G}_j]$$

$$-\frac{1}{2} A_{\mathrm{D}}(\mathscr{U}_j, \mathscr{U}_{j+1}) \cdot (\mathscr{U}_{j+1} - \mathscr{U}_j) \tag{20}$$

$$+\frac{1}{2} A_{\mathrm{D}}(\mathscr{U}_{j-1}, \mathscr{U}_j) \cdot (\mathscr{U}_j - \mathscr{U}_{j-1})$$

Since $\mathscr{U}_j = \mathscr{U}_0 + \delta\mathscr{U}_j$ and the assumption of odd–even perturbations writes $\delta\mathscr{U}_{j-1} = -\delta\mathscr{U}_j = \delta\mathscr{U}_{j+1}$ Equation (20) rewrites:

$$G(\mathscr{U}_j, \mathscr{U}_{j+1}) - G(\mathscr{U}_{j-1}, \mathscr{U}_j) = (A_{\mathrm{D}}(\mathscr{U}_j, \mathscr{U}_{j+1}) + A_{\mathrm{D}}(\mathscr{U}_{j-1}, \mathscr{U}_j)) \cdot \delta\mathscr{U}_j \tag{21}$$

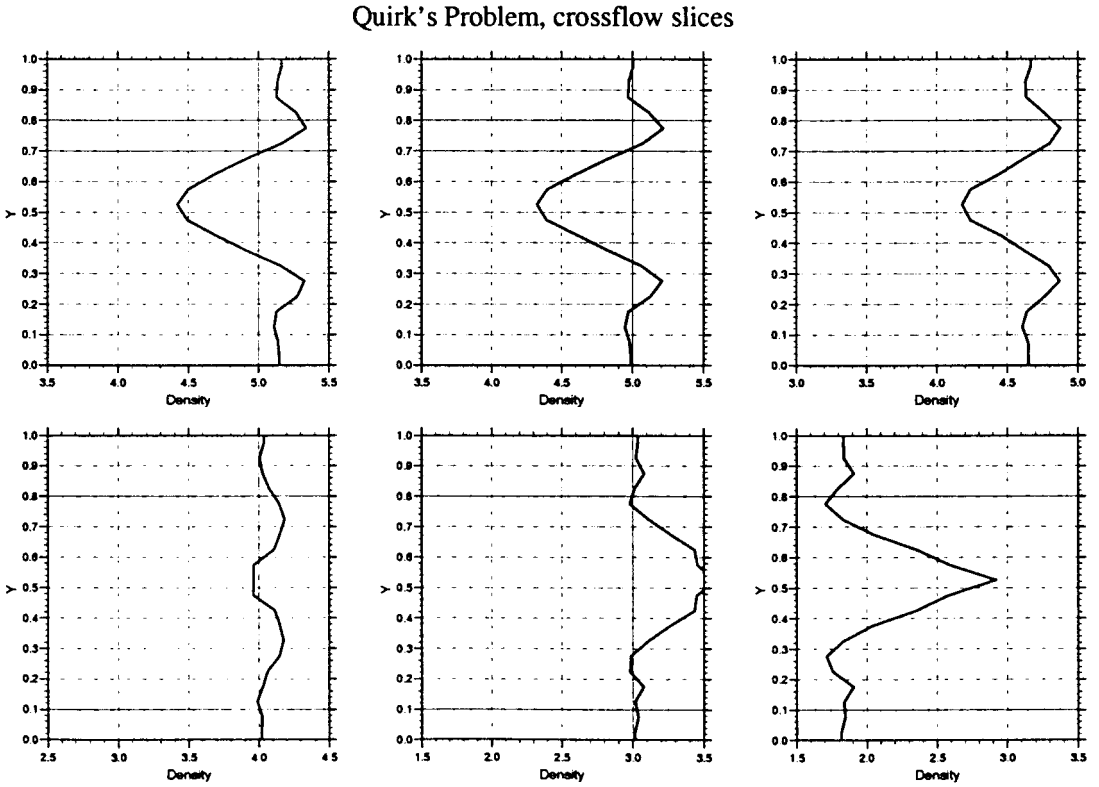

Figure 9. Density profiles within the shock for successive vertical grid lines around $x = 15$, AUSM-M scheme.

$A_D(\mathscr{U}_j, \mathscr{U}_{j+1})$ and $A_D(\mathscr{U}_{j-1}, \mathscr{U}_j)$ do not need to be developed. Otherwise, it would lead to second-order terms. Then, both dissipation matrices are approximated by $A_D(\mathscr{U}_0, \mathscr{U}_0)$. $\mathbb{G}$ matrix is directly expressed:

$$\mathbb{G} = 2A_D(\mathscr{U}_0, \mathscr{U}_0) \tag{22}$$

If any central scheme with matrix dissipation is required to exactly resolve contact discontinuities, the dissipation matrix $A_D(\mathscr{U}_L, \mathscr{U}_R)$ must satisfy the following property:

$$A_D(\mathscr{U}_L, \mathscr{U}_R) \cdot (\mathscr{U}_R - \mathscr{U}_L) = 0 \tag{23}$$

This simply means that $(\mathscr{U}_R - \mathscr{U}_L)$ is an eigenvector associated to a zero eigenvalue of A_D. Since $\mathbb{G} = 2A_D$, it implies that the amplification matrix $\mathbb{A}$ will necessarily have eigenvalues equal to 1. Therefore, this result show that for an artificial dissipation scheme (scalar or matricial), exact resolution of contact discontinuities leads to a marginally stable scheme.

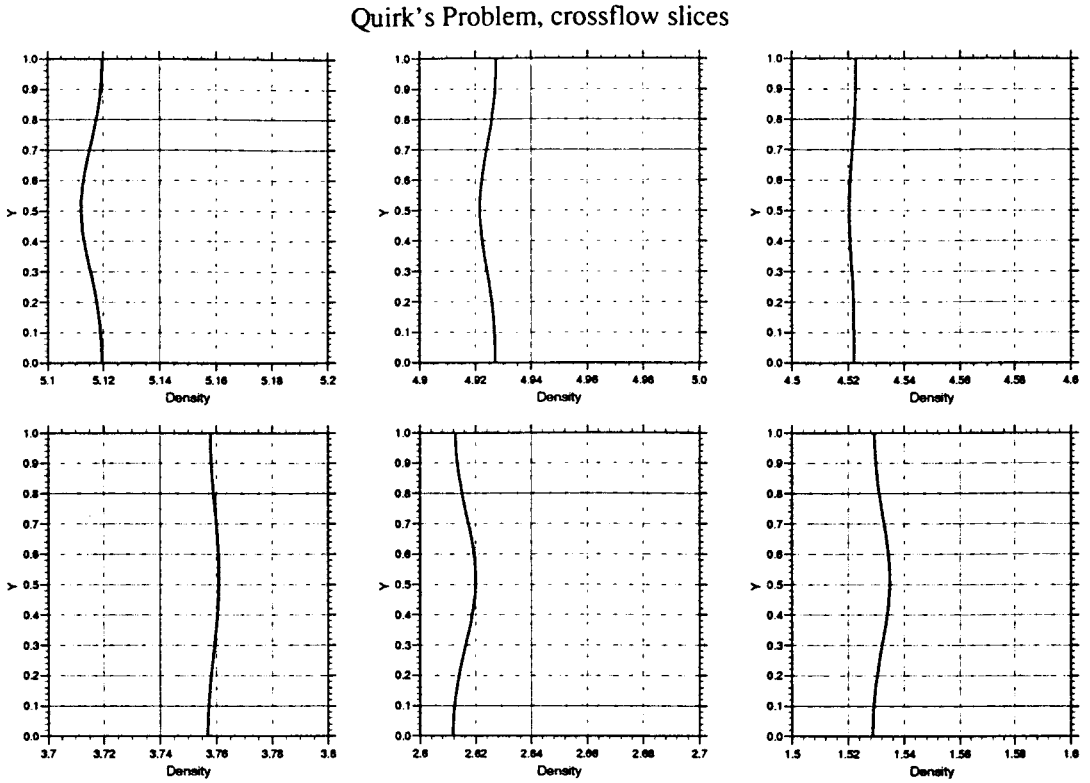

Figure 10. Density profiles within the shock for successive vertical grid lines around $x = 15$, EFM scheme.

Furthermore, any upwind scheme, after linearization, can be expressed as a central scheme with matrix dissipation. If the numerical flux is differentiable, the matrix A_D can be directly calculated with Jacobians of the numerical flux G:

$$A_D = \frac{\partial G}{\partial \mathcal{U}_L} - \frac{\partial G}{\partial \mathcal{U}_R} \tag{24}$$

Hence, previous results can be extended to all first-order schemes: if any upwind scheme provides accuracy on contact waves then it is marginally stable. In other words, any upwind scheme cannot simultaneously satisfy both the following properties: exact resolution of contact discontinuities and strict stability.

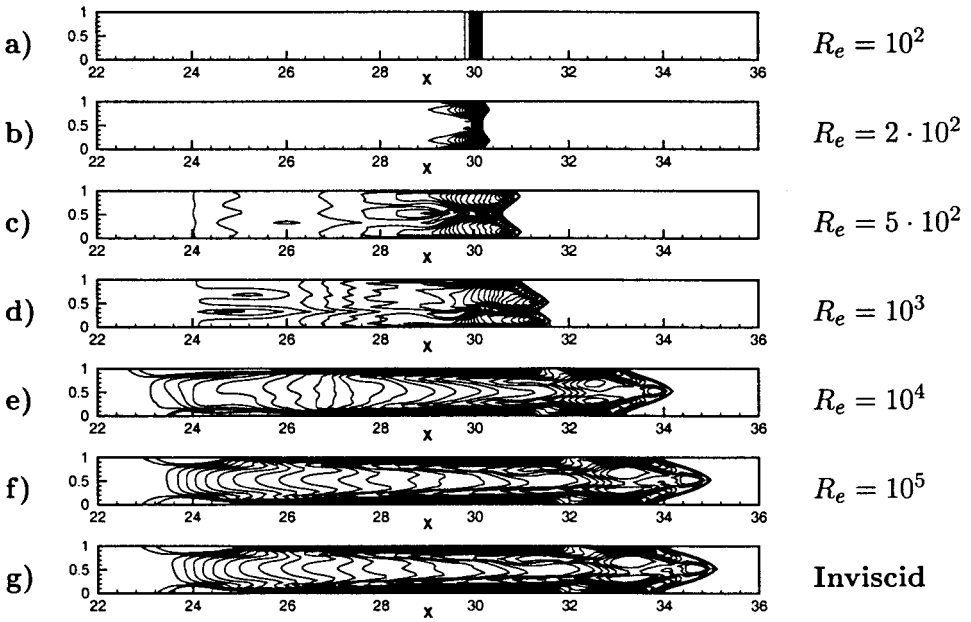

Figure 11. Effects of the natural viscosity, density contours.

9. VISCOUS COMPUTATIONS

According to the previous section, schemes which yield exact resolution of contact discontinuities are marginally stable and then might suffer from odd–even decoupling. Since this kind of accuracy is shown to be highly desirable for boundary layer computations, one might expect that the natural viscosity would be sufficient to damp oscillations generated downstream of the shock.

The following numerical results invalidate this expectation. In Figure 11, several viscous computations of Quirk's problem with Roe's scheme are presented. The Reynolds number *Re* is based on the duct width. In the different computations, all parameters are kept constant except the Reynolds number, which varies from one case to the other. In most computed cases, the natural viscosity is not sufficient to maintain straight shock profiles along the computation. The Reynolds number needs to decrease down to 10^2 which is a fairly low value for practical gas dynamics applications. This result shows that, in practice, one cannot rely on the natural viscosity to damp the numerical instability associated with the exact resolution of contact waves satisfied by an upwind method.

In practical applications where the Reynolds number is generally higher, the natural viscosity is not able to damp the odd–even decoupling of shocks. Then one can expect some difficulties using marginally stable schemes.

10. CONCLUDING REMARKS

The present analysis of odd–even decoupling has contributed to explain why Roe and EIM schemes fail in some situations. Applying the same analysis, the AUSM-M scheme although marginally stable, is observed to pass successfully Quirk's test. Nevertheless, this marginal behavior is consistent with the observed propagation of perturbations from the centerline along crossflow planes, and with the failing of the AUSM-M scheme on some other cases such as the DMR problem for high resolution computations.

Among the upwind methods considered in this study, the EFM scheme has been the only scheme which provides the desirable damping properties. Unfortunately, the EFM does not exactly resolve contact discontinuities. These features are shared by most FVS schemes [14]. In order to be used as a criterion, this analysis certainly needs to take into account perturbations due to source terms, the shock structure and streamwise fluxes contribution. Furthermore, the EFM scheme results reveal that strict stability is desirable to avoid these flaws.

The linear stability analysis has proved that any central scheme with matrix dissipation cannot simultaneously satisfy both properties, and the result is extended to any upwind scheme. In view of the proposed criteria and based upon the above-mentioned numerical observations, strict stability and exact resolution of contact discontinuities are not compatible. This might have heavy consequences on the development of future algorithms for the compressible Navier–Stokes equations, since natural viscosity cannot cure this flaw by itself.

APPENDIX A. NOMENCLATURE

a	sound speed
$\mathbb{A}$	amplification matrix
$\delta\mathscr{U}$	error vector
$\mathscr{G}$	physical flux vector
G	numerical flux vector
H	stagnation enthalpy
P	pressure
ρ	density
$\rho(\mathbb{A})$	spectral radius of $\mathbb{A}$
u, v	velocity components
$\mathscr{U}$	state vector

Subscripts

$_j$	transverse subscript
$_0$	reference values

Superscripts

^{n}	time step
$^\sim$	Roe average value

REFERENCES

1. Batten P, Clarke N, Lambert C, Causon DM. On the choice of waves speeds for the HLLC Riemann solver. *SIAM Journal on Scientific Computing* 1997; **18**(6): 1553–1570.
2. Coquel F, Liou MS. Hybrid Upwind Splitting (HUS) by a Field by Field Decomposition, NASA TM-106843, 1995.
3. Einfeldt B, Munz CD, Roe PL, Sjögreen B. On Godunov-type methods near low densities. *Journal of Computational Physics* 1991; **92**: 273–295.
4. Gressier J, Moschetta J-M. On the Pathological Behavior of Upwind Schemes, AIAA Paper 98-0110, January 1998.
5. Hirsch C. *Numerical Computation of Internal and External Flows*, *Computational Methods for Inviscid and Viscous Flows* (2nd ed.), vol. 2:. Wiley: New York, 1990.
6. Lax PD, Wendroff B. Systems of conservation laws. *Communications on Pure and Applied Mathemathics* 1960; **13**: 217–237.
7. Lin HC. Dissipations additions to flux difference splitting. *Journal of Computational Physics* 1995; **117**: 20–27.
8. Liou MS. Progress towards an Improved CFD Method: AUSM+, AIAA Paper 95-1701 CP, 1995.
9. Liou MS. Probing Numerical Fluxes: Mass Flux, Positivity and Entropy satisfying Property, AIAA Paper 97-2035, 1997.
10. Liou MS, Steffen CJ. A new flux splitting scheme. *Journal of Computational Physics* 1993; **107**: 23–39.
11. Macrossan MN, Oliver RI. A kinetic theory solution method for the Navier–Stokes equations. *International Journal for Numerical Methods in Fluids* 1993; **17**: 177–193.
12. Moschetta JM, Pullin DI. A robust low diffusive kinetic scheme for the Navier–Stokes equations. *Journal of Computational Physics* 1997; **133**(2): 193–204.
13. Osher S, Chakravarthy S. Upwind schemes and boundary conditions with applications to Euler equations in general geometries. *Journal of Computational Physics* 1983; **50**: 447–481.
14. Pandolfi M, D'Ambrosio D. Upwind methods and carbuncle phenomenon. In *Computational Fluid Dynamics 98*, *4th ECCOMAS*, vol. 1. Wiley: New York, 1998.
15. Peery KM, Imlay ST. Blunt body flow simulations. In AIAA Paper No. 88-2924, 1988.
16. Pullin DI. Direct simulation methods for compressible inviscid ideal gas flow. *Journal of Computational Physics* 1980; **34**: 231–244.
17. Quirk JJ. A contribution to the great Riemann solver debate. *International Journal for Numerical Methods in Fluids* 1994; **18**: 555–574.
18. Robinet J-Ch, Gressier J, Casalis G, Moschetta J-M. The carbuncle phenomenon: an intrinsic inviscid instability? In 22nd ISSW, July, 1999.
19. Roe PL. Approximate Riemann solvers, parameters vectors, and difference schemes. *Journal of Computational Physics* 1981; **43**: 357–372.
20. Sanders R, Morano E, Druguet M-C. Multi-dimensional dissipation for upwind schemes: stability and applications to gas dynamics. *Journal of Computational Physics* 1998; **145**: 511–537.
21. Toro EF, Spruce M, Speares W. Restoration of the contact surface in the HLL-Riemann solver. *Shock Waves* 1994; **4**: 25–34.
22. van Leer B. Towards the ultimate conservative difference scheme V. A second-order sequel to Godunov's method. *Journal of Computational Physics* 1979; **32**: 101–136.
23. Xu K. VKI Lecture Series 1998-03, February, 1998.

